Molecular Dynamics Simulations of Liquid Nitromethane

Dan C. Sorescu,*,†,‡ Betsy M. Rice,*,§ and Donald L. Thompson*,†

Department of Chemistry, Oklahoma State University, Stillwater, Oklahoma 74078, and The U. S. Army Research Laboratory, Aberdeen Proving Ground, Maryland 21005

Received: June 13, 2001; In Final Form: July 30, 2001

A classical potential consisting of both intramolecular and intermolecular (Buckingham and Coulombic) terms that was developed for the simulation of crystalline nitromethane has been used to investigate the dynamics of liquid nitromethane at various temperatures and pressures. The validation of the proposed potential model was done for a large number of static and dynamic properties including the heat of vaporization, the variation of density with temperature and pressure, the thermal expansion coefficient, the self-diffusion coefficients, the viscosity coefficient, the dielectric constant, the bulk modulus, and the variation of vibrational frequencies with pressure. The analyses performed using constant pressure and temperature and constant volume and temperature molecular dynamics simulations show that the potential accurately reproduces the structural properties of liquid nitromethane at ambient pressure in the temperature range 260−374 K as well as the compression effects up to 14.2 GPa.

I. Introduction

In a series of previous papers,[1−7] we have described the development and validation of a set of interaction potentials that can be used in atomic-level simulations to study the dynamics of a wide variety of energetic materials. In the initial study of this series, we developed a model to study nonreactive processes in the nitramine explosive RDX (1,3,5-hexahydro-1,3,5,-*s*-triazine).[1] That potential consists of atom−atom (6-exp) Buckingham potential terms plus electrostatic interactions. The Coulombic interactions were determined by fitting atom-centered partial charges to a quantum-mechanically determined electrostatic potential for a single RDX molecule for the structure corresponding to that in the crystal at ambient conditions. The remaining Buckingham parameters were adjusted to reproduce the experimental crystal structure of RDX at ambient conditions. This interaction potential was then used in molecular packing (MP) and isothermal−isobaric molecule dynamics (NPT-MD) simulations of the polymorphic phases of two other nitramine crystals: the polycyclic nitramine 2,4,6,8,10,12-hexanitrohexaazaisowurtzitane (HNIW or CL-20)[2] and the monocyclic nitramine octahydro-1,3,5,7-tetranitro-1,3,5,7-tetraazacyclooctane (HMX).[3] Additionally, we have shown that this interaction potential is transferable and can successfully reproduce the crystallographic structures and the lattice energies for a set of 30 mono- and polycyclic nitramine crystals[4] and 51 crystals containing nonnitramine molecules with functional groups common to energetic materials.[5]

A subsequent, more stringent assessment of the potential was accomplished through NPT-MD simulations of the energetic crystals RDX, HMX, HNIW, and PETN under hydrostatic compression conditions.[6]

Throughout this series of papers[1−6] the rigid-molecule approximation was assumed. As we have demonstrated, this model accurately describes the equilibrium structures of a variety of organic molecular crystals under ambient conditions and with moderate increases in pressure and temperature. However, the physical and chemical processes of energetic materials that are of most interest occur at high pressures and temperatures, where conformational molecular changes become important. Consequently, it is important that we extend the model to allow intramolecular motions, molecular deformation, and energy flow in the crystal. In a recent study, we undertook such a step and developed an intramolecular force field for prototypical explosive nitromethane, to be used in conjunction with the previously described transferable intermolecular potential model.[7] Nitromethane was selected for this first attempt at developing a fully flexible model of an energetic molecular crystal because numerous experimental investigations of its properties for a wide range of conditions have been reported, providing significant data for assessing the validity of the model potential. The analyses performed using NPT-MD and MP calculations showed that the proposed potential model is able to accurately reproduce the changes of the structural crystallographic parameters for the ranges of temperature (4.2−250 K) and pressure (0.3−7.0 GPa) studied. In addition, the calculated bulk modulus of nitromethane as well as the activation energy for internal rotation of the methyl group are in excellent agreement with the experimental results. Moreover, this potential correctly predicts the experimentally observed 45° change in the methyl group orientation in the high-pressure regime relative to the low-temperature configuration.

The validity of the intra- and intermolecular potentials depends on how well they predict the physical properties of other phases. Thus, in the present work, we investigate the transferability of the potential developed for crystalline nitromethane to the liquid phase of nitromethane by computing various physical properties of the liquid as functions of temperature and pressure. As in our study of solid nitromethane,[7] a motivation for the choice of liquid nitromethane for the present study is the existence of a number of experimental and theoretical studies in the literature[8−23] that provide a large amount of data for various physical properties of the liquid phase over wide ranges of temperature and pressure for comparisons.

* To whom correspondence should be addressed.
† Oklahoma State University.
‡ Current mailing address: Department of Chemistry, University of Pittsburgh, Pittsburgh, PA 15260.
§ The U. S. Army Research Laboratory.

10.1021/jp0122530 CCC: $20.00
Published on Web 09/14/2001

Among the properties we consider in this study are the heat of vaporization, the variation of density with temperature and pressure, the thermal expansion coefficient, the self-diffusion coefficients, the viscosity coefficient, the dielectric constant, the variation of some vibrational frequencies with pressure, the isothermal compressibility, and the bulk modulus.

In section II, we provide a brief description of the potential model, and a description of the computational details is given in section III. Section IV contains the results of the NPT-MD simulations and comparisons of the computed properties with the experimental data and other theoretical results available in the literature. The conclusions of the study are given in section V.

II. Potential Energy Functions

The intra- and intermolecular potentials used for simulation of liquid nitromethane are identical to those we used in MD studies of crystalline nitromethane.[7] Consequently, here we will present only the major characteristics of this potential. The intermolecular potential consists of the superposition of pairwise Buckingham and Coulombic potential terms of the form

$$V_{\alpha\beta}^{\text{inter}}(r) = A_{\alpha\beta}\exp(-B_{\alpha\beta}r) - C_{\alpha\beta}/r^6 + \frac{q_\alpha q_\beta}{4\pi\epsilon_0 r} \qquad (1)$$

where r is the interatomic distance between atoms α and β, q_α and q_β are the electrostatic charges on the atoms, and ϵ_0 is the dielectric permittivity constant of free space. The parameters $A_{\alpha\beta}$, $B_{\alpha\beta}$, and $C_{\alpha\beta}$ for various types of atomic pairs have been previously published[1] and have been used in the present study without change.

The intramolecular interactions are represented as a superposition of bond stretching, angle bending, and torsional potentials:

$$V_{\text{stretch}} = \sum_{i=1}^{6} D_{ei}\{[1 - \exp(-\beta_i(r_i - r_i^0))]^2 - 1\}$$

$$V_{\text{bend}} = \sum_{i=1}^{9} \frac{1}{2} k_i(\theta_i - \theta_i^0)^2$$

$$V_{\text{torsion}} = \sum_{i=1}^{7} V_{\Phi i}[1 + \cos(m\Phi - \delta)] \qquad (2)$$

The nine bending potentials correspond to the HCH, HCN, CNO, and ONO angles. The cosine-type torsional potentials describe the relative positions of the C−NO_2 atoms and the orientations of the H atoms relative to the C−N−O planes. Six of the torsional angles are defined by the HCNO dihedrals, and the seventh is defined by the N−O−O−C dihedral. The bond dissociation energies in eq 2 are taken from a previous study of nitromethane in the gas phase,[24] whereas the remaining set of values of the geometrical equilibrium parameters and force constants were parametrized using a quantum mechanical Cartesian force constant matrix to reproduce the gas-phase vibrational frequencies and the experimental barrier for the methyl group rotation. Details of the procedure used to evaluate the intramolecular terms as well as the complete list of the values of the potential parameters in eqs 1 and 2 are given in ref 7.

III. Computational Details

The dynamics of liquid nitromethane as functions of temperature and pressure have been investigated by using the potential described in eqs 1 and 2 in NPT-MD simulations. The Berendsen thermostat−barostat algorithm[25] as implemented in the program DL_POLY_2.0[26] was used to simulate the liquid at various temperatures and pressures. The equations of motion for the molecules and the simulation cell were integrated by using the Verlet leapfrog scheme.[27]

Most of the MD simulations have been done using cubic boxes containing 216 nitromethane molecules. The total energy of the system was calculated subject to the use of minimum-image periodic boundary conditions in all dimensions.[27] At ambient pressure, the interactions were determined between the sites (atoms) in the simulation box and the nearest-image sites within the cutoff distance of 12 Å, but in the simulations at higher pressures, the cutoff distance was decreased when necessary to ensure that it was always slightly smaller than half of the simulation box length. In all of these calculations, the Coulombic long-range interactions were handled using Ewald's method.[27]

In the production runs, the system was first equilibrated for a period of 50 ps (1 integration time step = 0.5 fs). The properties were then calculated by averaging over the next 100 ps. We have used longer trajectories (up to 600 ps) for the calculations of the dielectric properties because of the slower rate of convergence.

Several quantities that describe structural, energetic, spectroscopic, and transport properties of nitromethane have been obtained from these simulations. Specific details are provided in the next sections.

TABLE 1: Density, Heat of Vaporization, Diffusion Coefficient, and Shear Viscosity for Liquid Nitromethane as Functions of Temperature at Ambient Pressure

T (K)	density (g/cm^3)	ΔH_v (kJ/mol)	$D \times 10^{-9}$ (m^2/s)	η (mPa s)
		Experiments		
293.0	1.137[a]			
298.15		38.271[b]	2.39[c]	
374.4		33.992[d]		
		MD Calculations[e]		
255.0	1.149	42.845	0.648	
260.0	1.143	42.367	0.824	1.22
270.0	1.132	41.840	0.896	
290.0	1.103	40.419	1.238	
298.0	1.093	39.935	1.528	0.67
320.0	1.061	38.494	2.363	0.52
340.0	1.035	37.358	2.834	0.41
360.0	1.009	36.492	3.284	0.33
374.0	0.983	35.201	3.835	
400.0	0.959	34.192		
		Calculated, Alper et al.[f]		
300.0	1.107	39.748	1.52	
400.0		34.309		

[a] Reference 8. [b] Reference 9. [c] Reference 20. [d] Reference 10. [e] Present work. [f] Theoretical results reported in ref 11.

IV. Results and Discussions

1. Static Properties. We first calculated the static properties of liquid nitromethane as functions of temperature at ambient pressure as averages over 100 ps trajectories. The computed values of the density, the heat of vaporization (ΔH_v), diffusion coefficient (D), and shear viscosity (η) are given in Table 1; the available experimental values are also listed in the table for comparison.

The computed values of the density are given in column 2 of Table 1. The calculated density values (triangles) are compared to the available experimental data (squares) in Figure 1. At 290 K, the predicted density is 1.103 g/cm^3, which is about

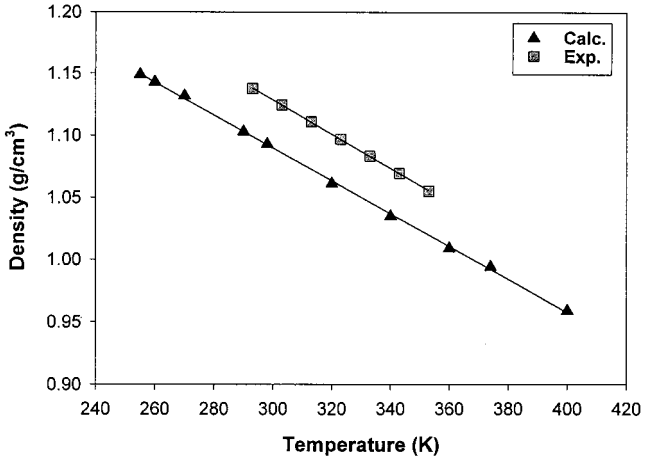

Figure 1. Comparison of the calculated density of liquid nitromethane with experimental data from ref 8. The solid lines represent linear least-squares fits to the points.

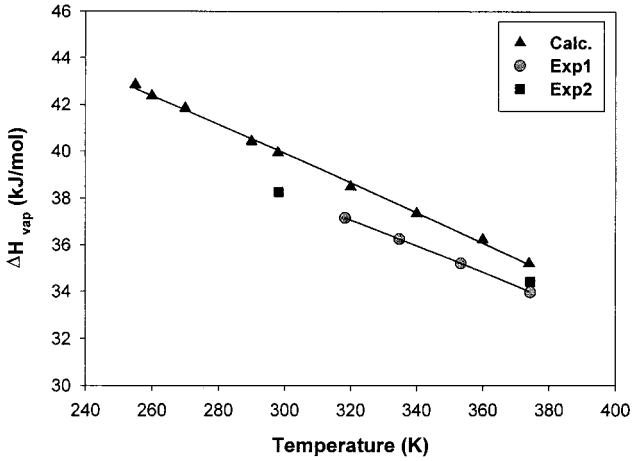

Figure 2. Variation of the predicted heat of vaporization for liquid nitromethane with temperature. The experimental data from ref 10 (denoted Exp1) as well as the data points (denoted Exp 2) at 298 (ref 9) and 374.4 K (ref 12) are shown for comparison.

2.9% smaller than the experimental value.[8] The overall density dependence is linear over the temperature interval studied, 255−374 K. A linear least-squares fit of the computed values gives $\rho_{calc}(T) = 1.486\,65 - 0.001\,323T$; see the straight line through triangles in Figure 1. A similar analysis was performed for the experimental data from ref 8 giving $\rho_{exp}(T) = 1.542\,32 - 0.001\,379T$ (see Figure 1). As shown by these equations and the results in Figure 1, the present potential predicts a similar variation of the liquid density with temperature for the entire range where experimental data are available.

The theoretical values obtained by Alper et al.[11] based on NPT-MD simulations with a classical force field developed specifically for liquid nitromethane are given in the last two rows of Table 1. The values of the parameters in that force field were adjusted iteratively until satisfactory agreement for the density, pair correlation function, heat of vaporization, and various vibrational frequencies were obtained at room temperature and ambient pressure.[11] At 300 K, their calculated density of 1.107 g/cm^3 is very close to the value predicted by our force field (1.093 g/cm^3 at 298 K). The difference is only 1.2%. This agreement is notable considering that our force field has not been fitted using any explicit information for the liquid phase. Rather the intermolecular portion (except for the partial atomic charges) was parametrized using information for a single nitramine crystal (i.e., RDX),[1] and the intramolecular portion was parametrized using only gas-phase information for nitromethane.[7]

The thermal expansion coefficient $\alpha = 1/V\,(\partial V/\partial T)_P$ can be readily obtained from the variation of the simulation box volume with temperature. A linear least-squares fit of the computed values of the volume leads to a temperature dependence of the form $V(T) = 12\,518.9116 + 25.380\,29T$ Å^3 from which an expansion coefficient of 1.26×10^{-3} K^{-1} at 298 K is determined. This value is slightly larger than the experimental average expansion coefficient of 1.205×10^{-3} K^{-1} given by Rabinovich[8] for the temperature range 293−363 K.

The heat of vaporization (ΔH_v) determined at various temperatures is given in column three of Table 1. These values have been evaluated from MD simulations according to the equation

$$\Delta H_{vap}(T) \approx -U_{int}(T) + RT \qquad (3)$$

where U_{int} is the total average intermolecular potential energy of the liquid. By using eq 3, we have assumed that the quantum correction terms related to the difference in intramolecular vibrational energy between the liquid state and the gas phase as well as the quantum correction that depends on the intermolecular vibrational modes of the liquid can be neglected.

The predicted values of ΔH_v are compared to the available experimental data in Figure 2. This figure includes the data collected between 318.3 and 374.4 K by McCullough et al.[10] (denoted as Exp1 in Figure 2), and the individual points at 298 K were determined by Jones and Giauque[9] and at 374.4 K were obtained by Pitzer et al.[12] (both are denoted as Exp2 in Figure 2). The computed value of ΔH_v at 298 K is in reasonable agreement (within 4.3%) with the experimental value.[9] The classical potential developed by Alper et al.[11] predicts a value for ΔH_v in excess of about 3.9% from the experimental value at this temperature. Alper et al.[11] calculated the heat of vaporization by considering only the negative of the calculated intermolecular potential energy. It is not clear if any thermal corrections were considered in their calculations. If these were not included, the error will be greater.

Following the method described by Majer et al.,[13] we fit the temperature dependence of the computed values of ΔH_v with the equation $A \exp(-\beta T_r)(1 - T_r)^\beta$ where $T_r = T/T_c$ with $T_c = 588$ K, the critical temperature of nitromethane. When the fit is performed to data generated for the temperature interval 320−374 K used in experimental investigations, the best-fit parameters are $A^{calc} = 55.764$ kJ/mol and $\beta^{calc} = 0.2780$. The values of the parameters obtained by fitting the experimental values are $A^{exp} = 53.33$ kJ/mol and $\beta^{calc} = 0.2732$ over the same temperature range.[13] The linear fit for the Exp1 set of data in Figure 2 is shown as a solid line through the points (circles). We have also performed a least-squares fit over the entire temperature interval, i.e., 255−374 K, (see the solid line and triangles in Figure 2) for the MD calculated values. The overall dependence is $\Delta H_v = 57.714 \exp(-0.3011T_r)(1 - T_r)^{0.3011}$. As can be seen from the results in Figure 2, the predicted temperature dependence of ΔH_v is in excellent agreement with that determined from the experimental data. Despite the slight differences in the magnitudes of the computed and measured values, the overall temperature dependences are in accord.

2. Structural Properties. The structural properties of liquid nitromethane have been investigated in terms of various site−site pair radial distribution functions (RDFs). These functions have been evaluated for correlation distances up to 12 Å (as limited by our choice of the cutoff distance for the intermolecular interactions) with a resolution of 0.05 Å. The computed

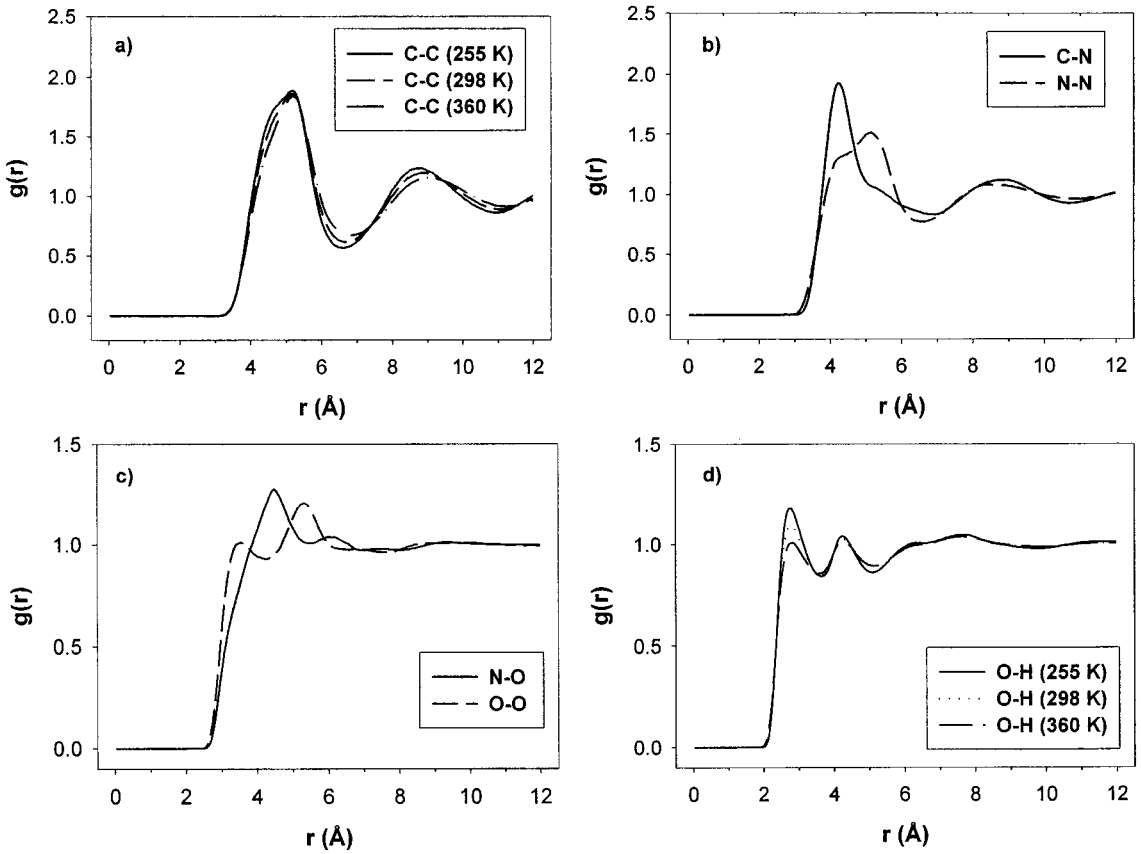

Figure 3. Radial distribution functions for the (a) C···C, (b) C···N and N···N, (c) N···O and O···O, and (d) O···H pairs at ambient pressure and $T = 298$ K (and $T = 255$ and 360 K for the C···C and O···H pairs).

distributions are shown in Figure 3. The RDF for the C−C pair (Figure 3a) shows that the first shell of a given nitromethane molecule is between 4 and 6 Å, whereas a second shell is positioned between 8 and 10 Å. This distribution remains almost unchanged with temperature in the range 255−360 K as illustrated in Figure 3a excepting a slight broadening of the bands and a small shift to larger distances of the positions of the peaks with increasing temperature. The integral up to the first minimum of the C−C RDF gives a coordination number of 12.8. This indicates that in the first coordination shell there are 12 nitromethane molecules. At 298 K, the first peaks for the C−C, C−N, and N−N RDFs are located at 5.2, 4.2, and 5.1 Å, respectively. For the C−C and C−N distributions, the first peak is well defined, but for the N−N case, the distribution is broader with almost a double-peak feature. The structure of the RDFs have been previously analyzed theoretically in two studies by Politzer and co-workers.[11,14] Their initial investigation,[14] based on a combined density functional MD method, predict that the first peaks in the RDFs for the C−C, C−N, and N−N pairs are located at approximately 5.2, 4.2, and 4.6 Å, respectively. Similar results for C−C and C−N pairs were computed in the second study[11] based on molecular simulations with a classical force field. The major difference observed in the second study is the presence of a broader distribution centered at about 4.8 Å for the N−N pair correlation function with a double-peak feature. These sets of results are similar to our RDFs (see Figure 3a,b). Also, the RDFs of the N−O and O−O atomic pairs presented in Figure 4c closely resemble the results reported by Alper et al.[11] Both the double-peak shape for the O−O RDF as well as the single peak structure for N−O distribution are similar to the results reported in ref 11. Finally, for the RDF of the O−H pair represented in Figure 3d, we observe a double peak structure at 2.8 and 4.3 Å. Alper et al.[11]

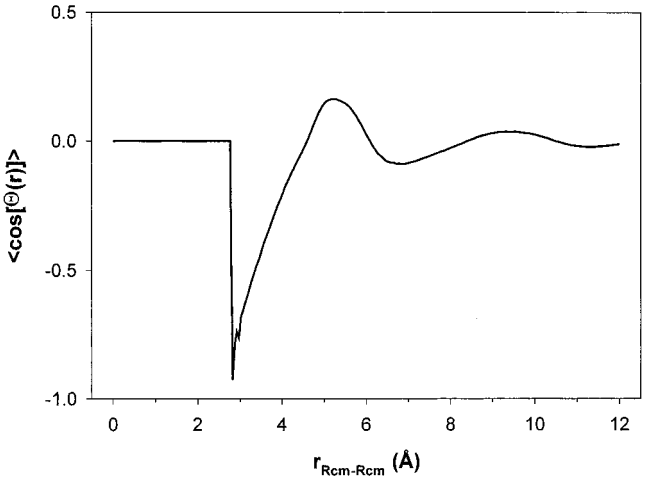

Figure 4. Average relative orientations of the molecular dipoles as a function of the distance between the molecular centers of mass (see eq 4). As expected, the dipoles align in opposite directions at short distances.

have obtained two peaks in the region 2−3 Å and an additional one at about 4.5 Å for this bond pair.

A limitation in the information provided by RDFs between different atomic pairs is due to the fact that the orientational characteristics are averaged. To have a better understanding of the orientational structure of the nitromethane molecules, we have calculated the angle distribution of the total dipole of the molecules. This quantity can be obtained as

$$\langle \cos(\theta(r)) \rangle = \left\langle \frac{\vec{\mu}_i \vec{\mu}_j}{\mu^2} \right\rangle \qquad (4)$$

where $\theta(r)$ is the angle between the dipole moments $\vec{\mu}$ of two molecules with molecular centers separated by the distance r. A typical distribution of the function $\langle\cos(\theta(r))\rangle$ averaged over the entire 100 ps trajectory at 298 K is shown in Figure 4. This plot shows that at short separation distances the most favorable configuration between two nitromethane molecules is antiparallel alignment of the dipoles.

3. Vibrational Properties. An additional property we have extracted from the analysis of MD simulations is the vibrational spectrum of liquid nitromethane. This has been obtained by computing the Fourier transform of the velocity autocorrelation function and is shown in Figure 5a. The individual peaks in the spectrum in Figure 5a can be identified approximately by using the power spectra of the velocity autocorrelation functions of the individual types of atoms, i.e., C, N, H, and O, which are given in Figure 5b−e. The calculated frequencies compare relatively well to those reported in ref 7, but in many instances, there are red shifts of 5−10% relative to gas-phase nitromethane. Exceptions are the high C−H stretching frequencies at 3095 and 2970 cm^{-1} which are almost unchanged from the gas-phase values of 3093 and 2961 cm^{-1} reported in ref 7. It is interesting to note that the spectrum of H atoms resembles the main qualitative features of the entire spectrum, except for the peak at 1547 cm^{-1}, which corresponds to the antisymmetric stretching mode of NO_2. Similarly, the spectrum of the O atoms given in Figure 5e also presents the main features of the entire spectrum except for the high-frequency C−H stretching modes. These characteristics have also been observed by Tuckerman and Klein[15] in an ab initio MD study of solid nitromethane. This indicates that the spectral features are not very sensitive to the phase. Additionally, in the same study,[15] it was suggested that a one-dimensional model of the methyl rotation would not accurately describe this motion. The similarity of our vibrational spectra to those obtained in ref 15 indicates that our choice for the functional description of the methyl group rotation around the CN axis based on the use of six HCNO torsional angles provides a satisfactory depiction of this motion.

4. Dynamical Properties. To determine the dynamical properties of liquid nitromethane, we have calculated the appropriate time correlation functions of various variables of the system.

An example is the autocorrelation function of the molecular center of mass linear velocity (VACF). This function, which provides information about translational motion of the molecules in the fluid, has been determined for ensembles of 216 molecules at various temperatures. The results are shown in Figure 6a. At 298 K, the correlation function rapidly goes to zero in about 0.2 ps, after which the function enters a negative region corresponding to a "cage effect" that extends up to 1.5 ps. After the negative peak the correlation function decays exponentially to zero. The existence of this negative region in the correlation function indicates the presence of a sequence of rebounding collisions, with surrounding molecules in the first coordination shell leading to a cage-like effect. The depth and position of the negative region of the autocorrelation function varies as function of temperature. For example, at $T = 255$ K, the minimum of −0.1135 is at 0.32 ps, whereas at 374 K, the minimum of −0.0380 is at 0.485 ps. The decrease of the negative minimum of the autocorrelation function with the temperature increase indicates enhancement of the diffusive character of the molecular motion.

The single exponential decay for the tail of the VACF is illustrated in more detail in the inset of Figure 6b, where we show a plot of the VACF and the corresponding fitted exponential (solid line) for times larger than 0.5 ps. It is clear that there are no systematic deviations between the two sets of data; thus, the time dependence of the VACF can be described as exponential with a time constant of 0.51 ps. For simple liquids, particularly for hard-disk ($d = 2$) and hard-sphere ($d = 3$) fluids, earlier MD simulations[28] have indicated that VACFs decay according to a power law, $t^{-d/2}$. A similar $t^{-3/2}$ dependence at very long times was predicted by generalized hydrodynamics theories.[29] However, the results of the present work indicate a different dependence for the tail of the VACF. A similar exponential dependence was observed by Daivis and Evans[30] for liquid butane.

Additional information about the dynamics of molecules in the liquid phase has been obtained by analyzing the rotational correlation times of specific vectors associated to the individual molecules. In particular, we have considered two vectors with their origins at the molecular centers of mass (CM); one is oriented toward the C atom of the molecule, and the other is perpendicular to the C−CM−O plane. Because the molecule has C_{2v} symmetry, the CM position is practically along the C−N bond. Additionally, the dipole moment of the molecules lies along this principal axis. So, for the purpose of present investigations, we consider one of the two versors ($\hat{\mathbf{u}}_i$) oriented along the C−N bond direction, whereas the other one is perpendicular to the C−N−O plane. From the time history of these two versors, we have evaluated the rotational correlation functions using the Legendre polynomial functions $P_l[\cos(\theta)]$ of rank l ($l = 1$ and 2)[31]

$$C_i^{(l)}(t) = \langle P_l[\cos\theta_i(t)]\rangle = \langle P_l(\hat{\mathbf{u}}_i(0)\cdot\hat{\mathbf{u}}_i(t))\rangle, \quad i = 1 \text{ and } 2 \quad (5)$$

The results of the Legendre autocorrelation functions of the first and second orders for the parallel ($\hat{\mathbf{u}}_1$) and perpendicular ($\hat{\mathbf{u}}_2$) versor are shown in Figure 7a,b, respectively. From these dependencies, the single molecule reorientational correlation times can be determined by numerical integration or by fitting these correlations with exponential functions of the form $A\exp(-t/\tau)$. The results in Figure 7 show that the variation of these correlation functions is quite slow. For this reason, we have used a combined method for evaluation of the correlation times. In this method, numerical integration was performed for each correlation function up to 10 ps at 298 K and 4 ps at 360 K, respectively. The rest of the correlation functions were fitted to an exponential function and the integrals were obtained analytically. The results are given in Table 2.

First we note that the calculated correlation times are larger for the tumbling motion than for the spinning motion. This is illustrated by plots of correlation functions for the tumbling (Figure 7a) and spinning motion (Figure 7b) as functions of time. Because of the large difference between the moments of inertia for rotation about the axis perpendicular to the plane of nitro group ($I_x = 85.59$ amu Å^2) and for rotation about an axis aligned along the C−N bond ($I_z = 48.23$ amu Å^2),[32] it is expected that the spinning motion will be more rapid than the tumbling motion leading to a smaller correlation time for the former. Additionally, we observe that rotational correlation times decrease with increasing temperature. This effect can be understood as being due to an increase of the orientational disorder with increasing temperature and consequently a less effective dipolar interaction that tends to align the neighboring pairs of molecules.

Finally, an indication about the type of reorientational motion in liquid nitromethane can be obtained from the correlation times τ^1 and τ^2, respectively. For a symmetric top molecule, the orientational relaxation time ratio for the dipole axis should be

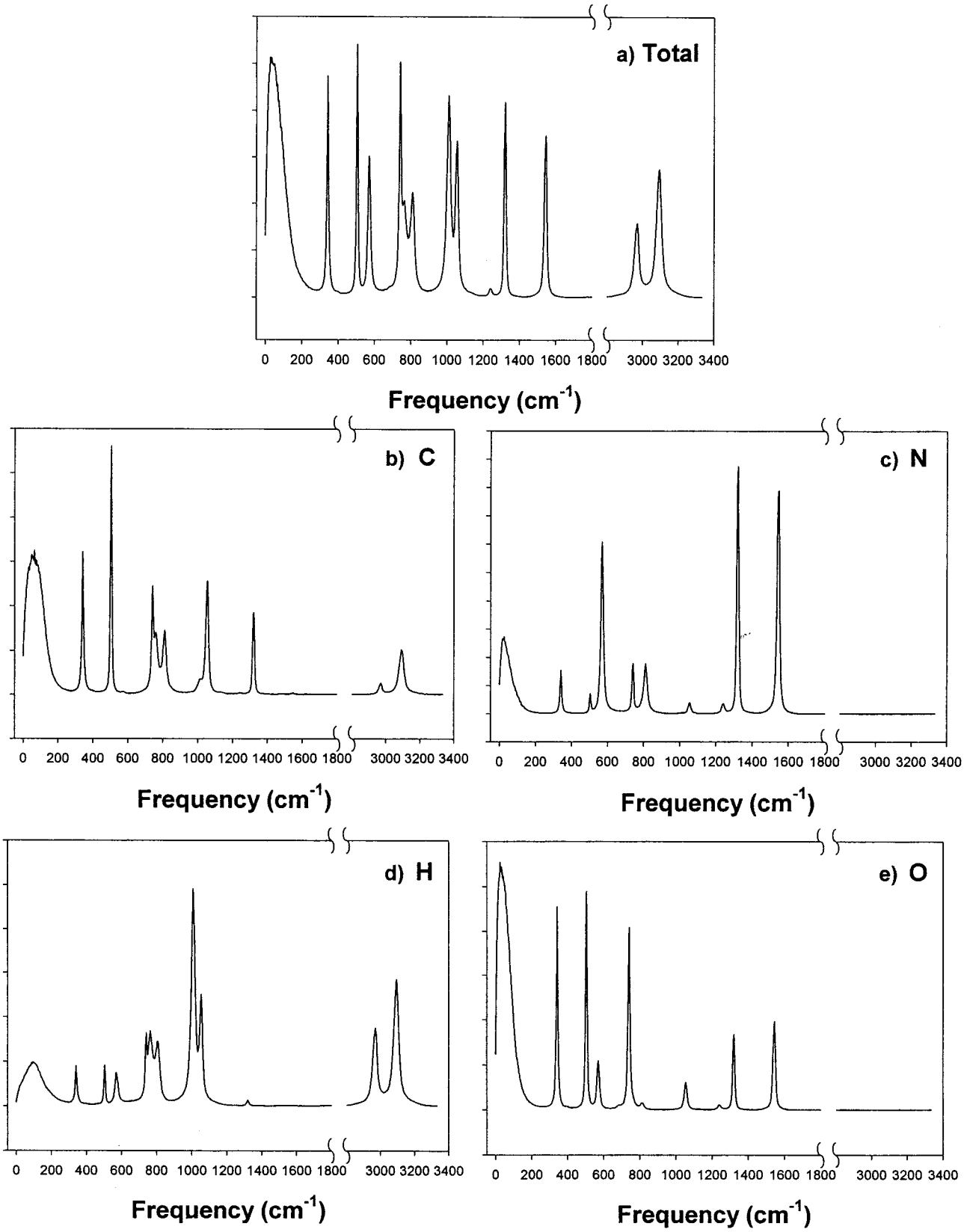

Figure 5. (a) Calculated composite power spectrum of liquid nitromethane at 298 K. The spectra for each type of atom are shown in other frames: (b) C, (c) N, (d) H, and (e) O.

equal to 3 on the basis of the different ranked tensorial properties.[31] The values from Table 2 for the tumbling motion indicate that $\tau_{\perp}^{1}/\tau_{\perp}^{2} = 2.98$, so the above condition is closely reproduced. Consequently, our results indicate that the rotational motion in liquid nitromethane is diffusional.

The calculated reorientational times are compared to the available experimental data in Table 2. Wang et al.[16] have determined a tumbling reorientational rate of 1.03 ps at 296 K using deuterium spin−lattice relaxation of nitromethane-d_3. Giorgini et al.[17] have analyzed the orientational processes in

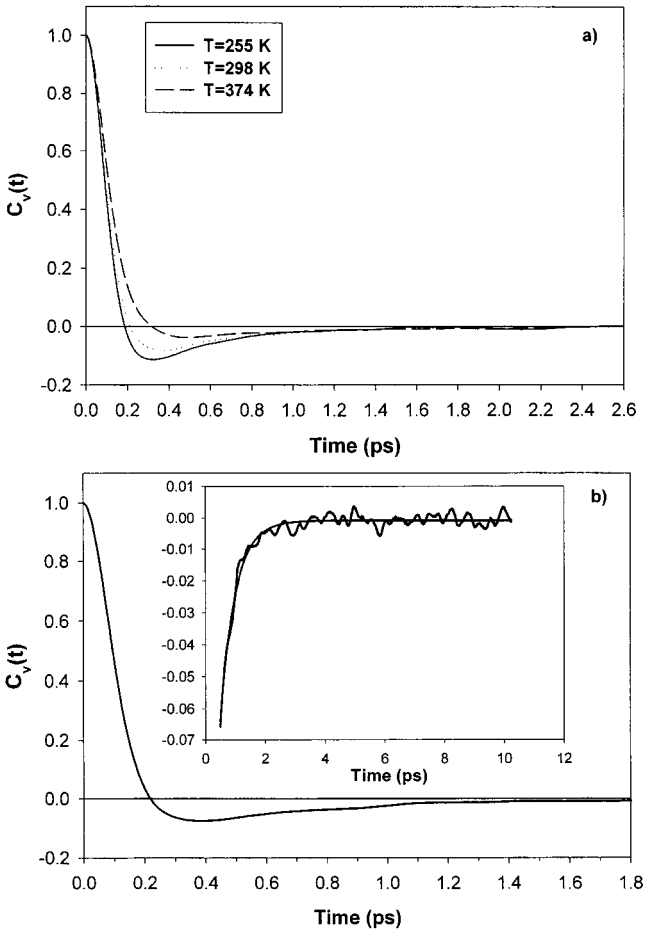

Figure 6. (a) Time correlation functions of the molecular center-of-mass linear velocities at 255, 298, and 374 K. (b) Detail of the velocity autocorrelation function at 298 K and of its tail (inset). In the inset figure, the solid line represents an exponential fit to the autocorrelation function for times larger than 0.5 ps.

liquid nitromethane based on depolarized light scattering and the transient optical Kerr effect. They have concluded that at longer times the orientational dynamics is diffusional, in agreement with our finding. At 293 K, the reorientation times for nitromethane were determined to be between 1.33 and 1.8 ps based on steady state (Raman and Rayleigh) and time-resolved (optical Kerr effect) spectroscopic experiments.[17] As indicated in Table 2, the experimental values for reorientational rates of the tumbling motion probed by Giorgini et al. experiments[17] are very close to our computed values.

A final analysis of the orientational properties of liquid nitromethane has been done by evaluation of the reorientation times of single molecule dipole moments (τ_D). In nitromethane, the dipole moment axis coincides with the C−N bond, and consequently the correlation times for individual molecules are expected to be similar to those obtained for the parallel versor $\hat{\mathbf{u}}_1$introduced above. As can be seen from the results presented in Table 2, both sets of values for $\tau^1{}_D$ and $\tau^1{}_\perp$ are very close, indicating the equivalence of the two descriptions.

5. Transport Properties. We have also investigated transport properties of liquid nitromethane. First, we computed the self-diffusion coefficient as a function of temperature. The self-diffusion coefficient D was calculated from the mean-square displacement of the molecular CM using the Einstein relation

$$D = \lim_{t\to\infty} \frac{\langle(\vec{r}(t) - \vec{r}(0))^2\rangle}{6t} \qquad (6)$$

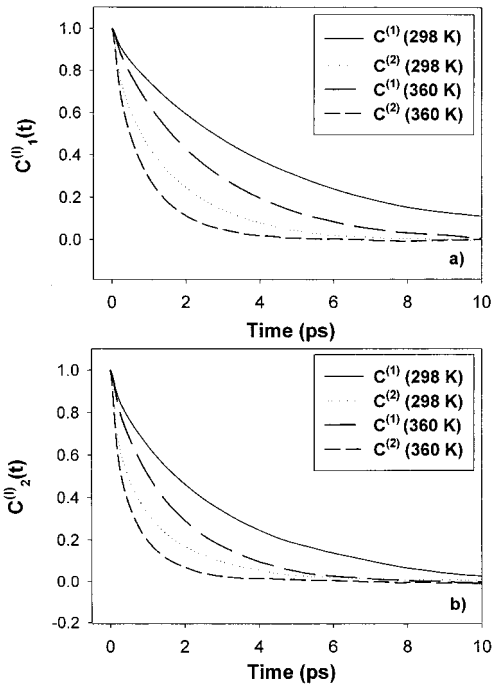

Figure 7. Time correlation functions of the first-order, $C^{(1)}$, and second-order, $C^{(2)}$, Legendre polynomials corresponding to (a) the parallel ($C^{(l)}{}_1$, $l = 1$ and 2) and (b) perpendicular ($C^{(l)}{}_2$, $l = 1$ and 2) versors at 298 and 360 K, respectively, as described in the text (see eq 5).

TABLE 2: Calculated Correlation Times (τ) of Liquid Nitromethane at 298 K for the Spinning ($\tau_\parallel$) and Tumbling ($\tau_\perp$) Motions Together with the Correlation Times for Single Molecule Dipole (τ_D) and for the Collective Dipole Moments (τ_Φ) (Available Experimental Data Are Also Given)

	$\tau^1{}_\parallel{}^a$	$\tau^2{}_\parallel$	$\tau^1{}_\perp$	$\tau^2{}_\perp$	$\tau^1{}_D$	$\tau^1{}_\Phi$
calc. (298 K)	2.86	1.08	4.15	1.39	4.22	5.32
calc. (360 K)	1.63	0.64	2.44	0.86	2.42	2.69
Exp 1 (NMR, 296 K)[b]				1.03		
Exp 2 (Raman, 293 K)				1.33		
Exp 3 (Rayleigh, 293 K)				1.40		
Exp 4 (OKE, 293 K)				1.80		
Exp 5 (Dielectric, 293 K)						4.1
(Dielectric, 333 K)						2.9
Exp 6						4.4

[a] The units for correlation times are ps. The indices 1 and 2 refer to the first- and second-order Legendre polynomials. [b] The experimental values are from NMR studies, ref 16 (Exp 1); Raman studies, ref 17 (Exp 2); Rayleigh scattering, ref 17 (Exp 3); transient optical Kerr effect (OKE) studies, ref 17 (Exp 4); dielectric relaxation experiments, ref 18 (Exp 5); additional data referenced in ref 17 (Exp.6).

where $\vec{r}(t)$ represents the position vector of the center of mass of a molecule at time t. The results are given in column 4 of Table 1.

In Figure 8, we compare our calculated values of D with the experimental results from two independent studies.[19,20] Overall, the calculated values are smaller than the experimental values, but they closely reproduce the temperature dependence found experimentally. The self-diffusion coefficients can all be described by an Arrhenius function ($D = D_0 \exp(-E_{diff}/kT)$, as shown by the straight line in Figure 8 obtained by a linear least-squares fit. The calculated values of the activation energy E_{diff} for the experimental sets of data Exp1[19] and Exp2[20] are 9.85 and 10.17 kJ/mol, respectively. The value 11.74 kJ/mol obtained by fitting our calculated values of the diffusion coefficient is only slightly higher. It is interesting to compare our values to those obtained from the MD simulations by Alper et al.[11] At

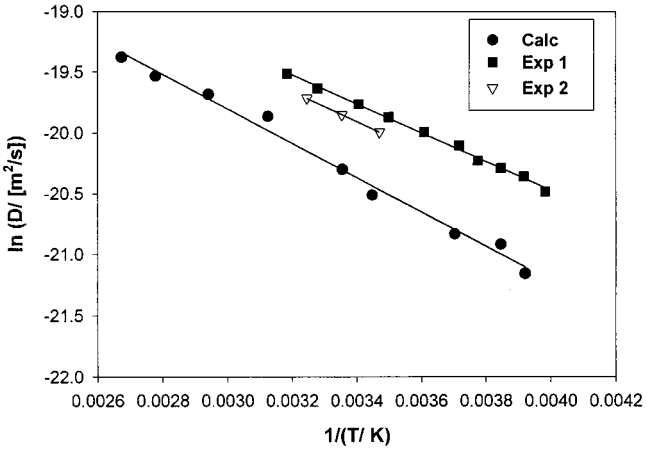

Figure 8. Comparison of the calculated diffusion coefficient D as a function of temperature with results from two independent studies (refs 19 and 20). The solid lines represent linear least-squares fits of the points.

300 K, they have found $D = 1.52 \times 10^{-9}$ m^2/s which is practically identical to our value of 1.528×10^{-9} m^2/s at 298 K.

We also computed the shear viscosity of liquid nitromethane. This quantity has been evaluated using a formalism similar to that described by Tironi and van Gunsteren.[33] Basically, the viscosity η is calculated from the displacement of the pressure tensor via the Einstein relation

$$\eta = \frac{1}{2}\frac{V}{k_B T}\lim_{t\to\infty}\frac{\mathrm{d}}{\mathrm{d}t}\langle \Delta P^2_{\alpha\beta}(t)\rangle \tag{7}$$

where

$$\Delta P_{\alpha\beta}(t) = \int_0^t P_{\alpha\beta}(t')\,\mathrm{d}t' \tag{8}$$

Here $P_{\alpha\beta}$ are the off-diagonal elements ($\alpha,\beta = x, y, z$) of the pressure tensor

$$P_{\alpha\beta}(t) = \frac{1}{V}\left\{\sum_i \frac{p^i_\alpha(t)p^i_\beta(t)}{m_i} + \sum_{i<j} F^{i,j}_\alpha(t)[r^i_\beta(t) - r^j_\beta(t)]\right\} \tag{9}$$

where p^i_α is the α component of the momentum for particle i and $F^{i,j}_\alpha$ is the α component of the force exerted on particle i by particle j.

The off-diagonal elements of the pressure tensor, eq 9, were saved at every step during trajectory simulations. Further improvement in the statistics was obtained by averaging over all three off-diagonal components of the pressure tensor. The calculated values of the viscosity coefficient are plotted as a function of temperature in Figure 9. At 298 K, the predicted value of the viscosity coefficient is 0.67 mPa s. This value is very close to the experimental values of 0.63 (ref 21) and 0.673 mPa s (ref 8). The results in Figure 9 illustrate that the viscosity coefficient obeys the Arrhenius equation: $\eta = \eta_0 \exp(E_{vis}/kT)$. A linear least-squares fit of the calculated values given in Figure 9 gives $\ln(\eta) = -4.4704 + 1215.8/T$ mPa s (shown by the solid line in Figure 9) over the temperature range 260−360 K, which is in accord with the experimental[22] result $\ln(\eta) = -3.989 + 1042/T$ mPa s (shown by the dashed line in Figure 9) for the temperature range 273−360 K. Both the magnitudes and temperature dependence of the computed results are in very close agreement with those of the experiment.

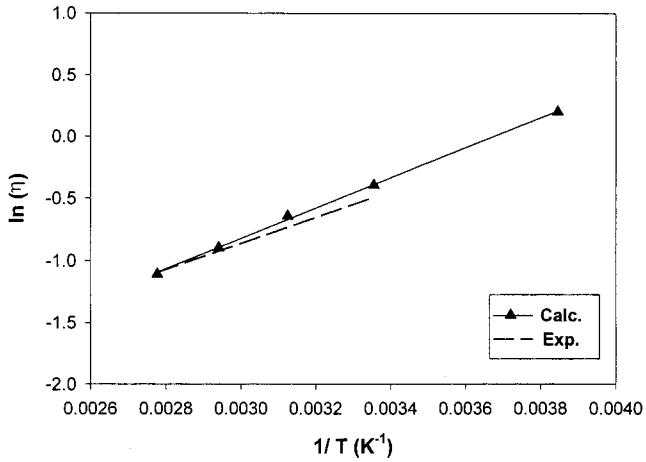

Figure 9. Variation of the viscosity coefficient with temperature. The solid line represents a linear least-squares fit of the calculated points. The dashed line is based on the experimental results given in ref 22.

Eyring[34] pointed out that for dense fluids the viscosity activation energy ΔE_{vis} is proportional to the energy of vaporization, $\Delta E_{vap} = n\Delta E_{vis}$, where $2 \le n \le 5$. Using the values for ΔE_{vap} given in Table 1 and the value of ΔE_{vis} determined above, we obtain $n = 3.95$.

With regard to the calculated viscosity coefficient, several types of correlations with the other dynamic properties such as the diffusion coefficients or relaxation rates are possible. For example, on the basis of depolarized light scattering and optical Kerr effect (OKE) measurements of the reorientational times in nitromethane, Giorgini et al.[17] have confirmed the existence of a linear dependence for the reorientation time on η/T ratio, $\tau = C\eta/T + \tau_0$, with the slope factor $C = 0.39$ (K ps/cP). Using the values of the $\tau^2_\perp$ rates for the tumbling motion together with the calculated viscosity coefficients at 298 and 360 K, we obtain a slope factor $C = 0.398$ (K ps/cP) and a positive intercept τ_0. Despite the limited results used in the analysis the slope of predicted and experimental curves are practically identical.

A second type of correlation we have analyzed is related to the relationship between the shear viscosity and the diffusion constant. Such a correlation can be represented as

$$\eta = K\frac{\rho T}{D} \tag{10}$$

where K is a proportionality constant. If we take as a reference the value of viscosity η_0 at a given temperature T_0 where the diffusion coefficient is D_0, it follows that

$$\eta = \eta_0\frac{\rho}{\rho_0}\frac{T}{T_0}\frac{D_0}{D} \tag{11}$$

We have evaluated the viscosity coefficient as a function of temperature, using the results calculated at 340 K as a reference. The calculated results based on eq 11 are shown as solid triangles in Figure 10, and the original values determined from the MD simulations are shown as open triangles. Clearly, the two sets of values are very close, indicating the validity of eq 10. The major advantage of using eq 10 is that it allows the evaluation of a collective property of the system such as the shear viscosity, using a single-molecule property such as the diffusion coefficient. The latter quantity converges at a higher rate than the former.[28]

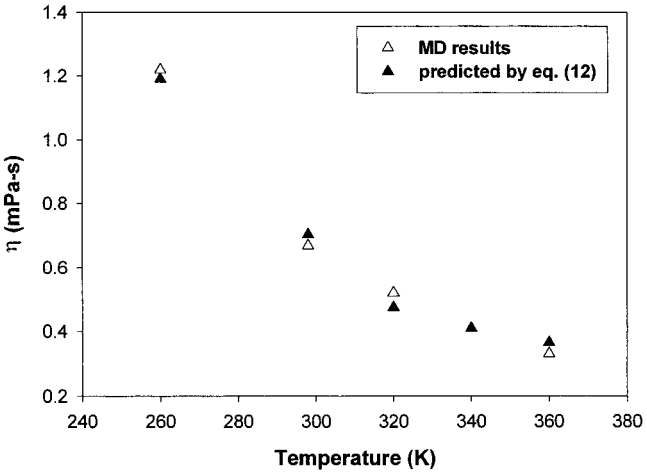

Figure 10. Shear viscosity as a function of temperature. The MD results (open triangles) are compared with the values computed by using eq 11 with the MD value at 340 K taken as the reference.

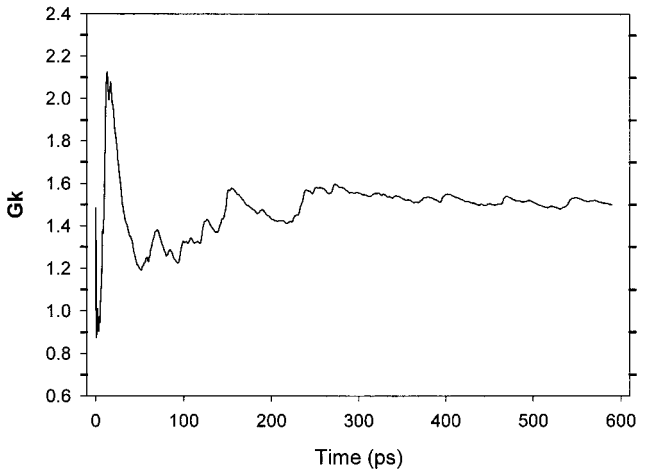

Figure 11. Time dependence of the cumulative time average factor G_k, eq 13.

6. Dielectric Properties. For a molecular fluid, the static relative dielectric constant ϵ_r can be evaluated using the G_k factor[35] based on the relation

$$\epsilon_r = 1 + \frac{1}{3\epsilon_0}\frac{N}{V}\frac{G_k\langle\vec{\mu}^2\rangle}{k_B T} \tag{12}$$

where ϵ_0 is the dielectric constant of the vacuum, $\vec{\mu}$ is the dipole moment of the molecule, and N is the number of molecules in volume V. The angular bracket $\langle\rangle$ denotes an ensemble average, and the factor G_k is defined as

$$G_k = \frac{\langle\vec{M}^2\rangle}{N\langle\vec{\mu}^2\rangle} \tag{13}$$

where $\vec{M} = \sum_{i=1}^{N}\vec{\mu}_i$ is the total dipole moment of the N molecules in the simulation box. Equation 13 indicates that the G_k factor is proportional to the ratio of the mean-squared total dipole to the mean-squared molecular dipole moment.

We have evaluated the G_k factor in an NVT simulation at 298 K and atmospheric pressure for a trajectory of 600 ps. As can be seen in Figure 11, it is necessary to use such a long trajectory because of the slow rate of convergence of the G_k factor. Indeed, for about 275 ps, there are some large fluctuations in the values of the G_k factor, but after which, the cumulative average starts to decrease and the G_k factor begins to converge. The dielectric constant obtained by using eqs 12 and 13 is 25.9, which is extremely close to the value of 26.44 obtained theoretically by Alper et al.[11] However, both values are only in fair agreement with the experimental constant of 37.27.[36] A major reason for this difference is probably due to the neglect of electronic polarizability in the potential models.

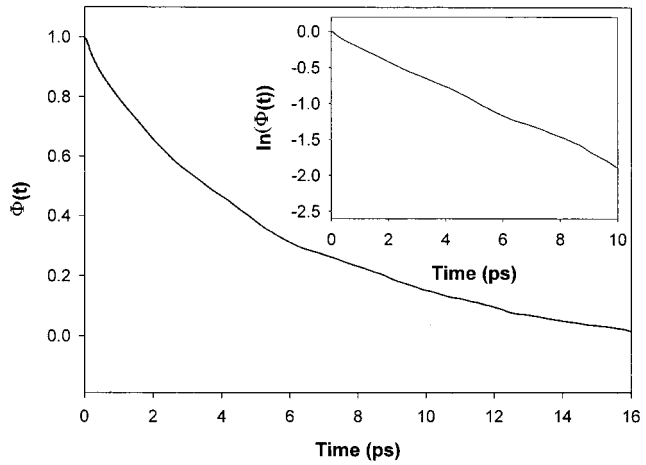

Figure 12. Time variation of the normalized autocorrelation function of the total dipole moment of the system. The inset indicates a semilogarithmic plot of the correlation function over the first 10 ps.

Additional insight in the dynamics of the dielectric medium has been obtained by investigation of the relaxation of the collective orientational ordering. This can be obtained from the autocorrelation function $\Phi(t)$ of the total dipole moment $\vec{M}$ of the simulation box fitted to an exponential dependence:

$$\Phi(t) = \frac{\langle\vec{M}(t)\cdot\vec{M}(0)\rangle}{\langle M^2(0)\rangle} = e^{-t/\tau_\Phi} \tag{14}$$

The knowledge of the function $\Phi(t)$ provides information about the frequency-dependent dielectric constant.[35] A normalized autocorrelation function of the total dipole moment of the system obtained at 298 K is presented in Figure 12. Table 2 contains the relaxation times obtained from the slopes of the logarithmic dependencies of the function $\Phi(t)$ at 298 and 360 K. The experimental relaxation times τ_Φ are also given in the last column of Table 2 for comparison. The agreement between the predicted and measured values is good. Moreover, our results also predict the correct decrease of the relaxation rates with temperature. At 360 K, τ_Φ decreases to 2.9 from the value of 5.4 at 298 K. A similar decrease, 4.1 at 298 K to 2.9 at 333 K, is observed experimentally.[18]

7. Pressure Effects. Finally, we have investigated the influence of hydrostatic compression on some of the physical and spectroscopic properties of nitromethane. These properties have been obtained from NPT simulations at 298 K and for pressures up to 14.2 GPa. The calculated values of the density and diffusion coefficient at various pressures are given in Table 3, whereas the variation of the specific volume (υ) with pressure is given in Figure 13.

For the low-pressure regime below 0.5 GPa, the variation of the specific volume with pressure is linear, but above this pressure, the rate of volume change decreases rapidly with the increase of pressure. This variation can be explained by the rapid increase in the repulsion between the molecules. The region of linear variation of volume with pressure gives an isothermal compressibility $k_T = -(1/V)\,(\partial V/\partial p)_T$ of 6.2×10^{-10} Pa^{-1} at 298 K.

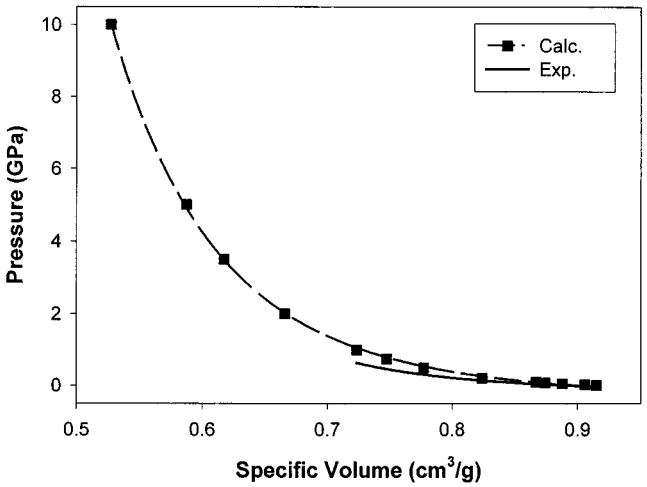

Figure 13. Comparison of the calculated $P-V$ isotherm with the data derived from ref 23.

TABLE 3: Calculated Density and Diffusion Coefficients for Liquid Nitromethane as Function of Pressure at 298 K

P (GPa)	ρ (g/cm^3)	$D \times 10^{-9}$ m^2/s
0.025	1.1036	1.2817
0.050	1.1261	1.1143
0.075	1.1439	0.9310
0.100	1.1533	1.0548
0.200	1.2137	0.5650
0.500	1.2865	0.3760
0.750	1.3376	0.1856
1.000	1.3817	0.1305
2.000	1.5014	0.0379
3.500	1.6193	0.0036
5.000	1.7025	0.0012
10.000	1.8962	0.0004
14.200	2.0107	0.0000

The strong intermolecular interactions experienced by the molecules upon compression cause large changes in the diffusion coefficient. As indicated by the results in Table 3, there is a sharp decrease in the diffusion coefficient for pressures above 0.5 GPa. This indicates that at these pressures that nitromethane is crystalline. Previous experimental studies[37,38] have indicated that the equilibrium crystallization pressure for liquid nitromethane at 298 K is about 0.4 GPa. In the crystalline phase and for pressures below 0.6 GPa, the methyl group is freely rotating. At intermediate pressures between 0.6 and 3.5 GPa, the rotation of methyl group is hindered, whereas for pressures above 3.5 GPa, the orientation of the methyl group becomes fixed. That the molecular motion is essentially frozen above 3.5 GPa is clearly apparent from our calculated values of the diffusion coefficient.

From the calculated $P-V$ data presented in Figure 13, the isothermal bulk modulus B_0 at zero pressure can be obtained using the Murnaghan equation[39]

$$P(V) = \frac{B_0}{B_0'}\left[\left(\frac{V_0}{V}\right)^{B_0'} - 1\right] \qquad (15)$$

In eq 15, V is the volume at pressure P, V_0 is the volume at $P = 0$, B_0 is the bulk modulus at $P = 0$, and $B_0' = \mathrm{d}B_0/\mathrm{d}P$. A least-squares fit of our calculated values for pressures up to 1 GPa leads to a value of $B_0 = 1.40$ GPa and $B_0' = 8.272$. In Figure 13, we also compare our calculated $P-V$ isotherm with the available data in the literature.[23] Particularly, we present in this plot the recent results obtained by Winey et al.[23] for the isothermal compression of nitromethane up to 1.0 GPa. Over this pressure range, they obtained $B_0^{(\mathrm{exp})} = 1.32$ GPa and $B_0'^{(\mathrm{exp})} = 7.144$.[23] These values are very close to our calculated values, indicating that our potential predicts a compression dependency similar to that observed experimentally, at least in the region of low pressures.

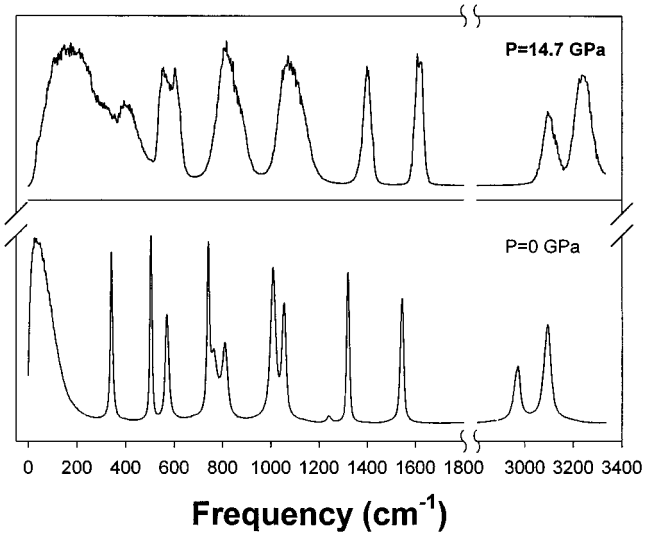

Figure 14. Comparison of the composite power spectrum at ambient pressure (lower frame) and at 14.2 GPa (upper frame).

The strong intermolecular interactions existent at high compressions are expected to influence the vibrational properties of nitromethane. To investigate this point, we have computed the composite power spectrum of nitromethane compressed at 14.2 GPa, which is shown in the upper frame of Figure 14. For comparison, the spectrum at ambient pressure is shown in the lower frame of Figure 14. Several effects are apparent from these plots. There are large shifts in the vibrational frequencies with the increased in pressure because of the effects of the strong intermolecular forces upon compression. These shifts correspond to mode hardening for all vibrational frequencies. The shifts are strongly dependent on the type of mode. For example, the shifts in the C−N stretching mode and NO_2 stretch/CH_3 bend modes are 49 and 62 cm^{-1}, respectively, whereas shifts in the C−H stretching modes are as large as 124 cm^{-1}. These effects indicate selective enhancement of the intermolecular interactions with modifications of the internal bonds. The effect is largest for the C−H modes as these modes harden the most.

In addition to the frequency shifts, there is significant broadening of the spectral lines. The broadening is particularly large for the case of the CH_3 stretching modes. Several factors can be responsible for this. First, there might be a distribution of bond strengths because of different local environments of the molecules. Also, the vibrational lifetimes can decrease because of increased coupling of the vibrational modes. It is important to note that the type of effects, i.e., frequency shifting and line broadening, observed in these simulations have also been found in the experimental studies.[40] Using time-resolved Raman spectroscopy, Pangilinan and Gupta[40] have analyzed the spectral properties of nitromethane shocked to 140 kbar. They observed a large shift of about 90 cm^{-1} for C−H stretching modes, whereas the C−N stretching vibration undergoes a shift of only about 50 cm^{-1}, and these shifts take place with large broadenings and intensity changes of the bands. This is qualitatively similar to what we observe in our computed results.

V. Conclusions

We have investigated the physical properties of liquid nitromethane by using MD simulations with a previously developed classical potential that includes intra- and intermolecular motions.[7] The results obtained with this potential in NPT-MD simulations over the temperature range 255−374 K at ambient pressure show that the model gives good agreement with experimental data for a large number of physical properties. For a more comprehensive test of the potential, we have considered both static and dynamic properties of liquid nitromethane, spectral properties, transport, and dielectric properties. Also, the investigations included calculations of the density, self-diffusion coefficient, and spectral properties of nitromethane under hydrostatic compression for pressures up to 14.2 GPa. Agreement with experimental data is generally quite good; however, the model gives less accurate predictions of the dielectric permittivity of liquid nitromethane. This is probably due to the lack of polarization effects in the intermolecular interactions. Our results were similar to those computed by Alper et al.[11] using a force field developed specifically to describe the properties of the liquid phase of nitromethane. Our potential was not specifically designed or parametrized to fit results for the liquid; however, as this and our previous study[7] show, it is generally accurate for both the solid and liquid phases. Furthermore, the intermolecular potential used here has been shown to describe a wide range of molecular solids.[1−6]

The success of the present potential model to describe the prototypical explosive, nitromethane, in both the solid[7] and liquid phases as well as it reliability in predictions for a large number of important energetic materials[1−6] provides incentive to extend it to applications such as solid−liquid-phase transitions, energy transfer, and reactions in condensed phases.

Acknowledgment. D.L.T. gratefully acknowledges support by the U. S. Army Research Office under Grant No. DAAD19-01-1-0022.

References and Notes

(1) Sorescu, D. C.; Rice, B. M.; Thompson, D. L. *J. Phys. Chem*. **1997**, *B101*, 798.
(2) Sorescu, D. C.; Rice, B. M.; Thompson, D. L. *J. Phys. Chem*. **1998**, *B102*, 948.
(3) Sorescu, D. C.; Rice, B. M.; Thompson, D. L. *J. Phys. Chem.* **1998**, *B102*, 6692.
(4) Sorescu, D. C.; Rice, B. M.; Thompson, D. L. *J. Phys. Chem.* **1998**, *A102*, 8386.
(5) Sorescu, D. C.; Rice, B. M.; Thompson, D. L. *J. Phys. Chem.* **1999**, *A103*, 989.
(6) Sorescu, D. C.; Rice, B. M.; Thompson, D. L. *J. Phys. Chem.* **1999**, *B103*, 6783.
(7) Sorescu, D. C.; Rice, B. M.; Thompson, D. L. *J. Phys. Chem.* **2000**, *B104*, 8406.
(8) Rabinovich, I. B. *Influence of Isotopy on the Physico-Chemical Properties of Liquids*; Consultants Bureau: New York, 1970.
(9) Jones, W. M.; Giauque, W. F. *J. Am. Chem. Soc*. **1947**, *69*, 983.
(10) McCullough, J. P.; Scott, D. W.; Pennington, R. E.; Hossenlopp, I. A.; Waddington, G. *J. Am. Chem. Soc*. **1954**, *76*, 4791.
(11) Alper, H. E.; Abu-Awwad, F.; Politzer, P. *J. Phys. Chem*. **1999**, *B103*, 9738.
(12) Pitzer, K. S.; Gwinn, W. D. *J. Am. Chem. Soc*. **1941**, *63*, 2419.
(13) Majer, V.; Svoboda, V.; Kehiaian, H. V. *Enthalpies of Vaporization of Organic Compounds: A Critical Review and Data Compilation*; Blackwell Scientific Publications: Oxford, 1985.
(14) Seminario, J. M.; Concha, M. C.; Politzer, P. *J. Chem. Phys*. **1995**, *102*, 8281.
(15) Tuckerman, M. E.; Klein, M. L. *Chem. Phys. Lett*. **1998**, *283*, 147.
(16) Wang, K. S.; Yuan, P.; Schwartz, M. *Spectrochim. Acta* **1992**, *48A*, 993.
(17) Giorgini, M. G.; Foggi, P.; Cataliotti, R. S.; Distefano, M. R.; Morresi, A.; Mariani, L. *J. Chem. Phys.* **1995**, *102*, 8763.
(18) Madan, M. P. *Can. J. Phys*. **1987**, *65*, 1573.
(19) Price, W. S.; Ide, H.; Arata, Y. *J. Chem. Phys*. **2000**, *113*, 3686.
(20) Holz, M.; Mao, X.; Seiferling, D. *J. Chem. Phys*. **1996**, *104*, 669.
(21) van Velzen, R. D.; Cardozo, R. L.; Lagenkamp, H. *Liquid Viscosity and Chemical Constitution of Organic Compounds: A New Correlation and a Compilation of Literature Data*; Euratom, 4735e; Joint Nuclear Research Centre: Ispra Establishment, Italy, 1972.
(22) Reid, R. C.; Prausnitz, J. M.; Poling, B. E. *The Properties of Gases & Liquids*, 4th ed.; McGraw-Hill Book Company: New York, 1987.
(23) Winey, J. M.; Duvall, G. E.; Knudson, M. D.; Gupta, Y. M. *J. Chem. Phys.* **2000**, *113*, 7492.
(24) Rice, B. M.; Thompson, D. L. *J. Chem. Phys*. **1990**, *93*, 7986.
(25) Berendsen, H. J. C.; Postma, J. P. M.; van Gunsteren, W.; DiNola, A.; Haak, J. R. *J. Chem. Phys.* **1984**, *81*, 3684.
(26) DL_POLY is a package of molecular simulation routines written by W. Smith and T. R. Forester, copyright The Council for the Central Laboratory of the Research Councils, Daresbury Laboratory at Daresbury, Nr. Warrington, 1996.
(27) Allen, M. P.; Tindesley, D. J. *Computer Simulation of Liquids*; Oxford University Press: New York, 1989.
(28) Haile, J. M. *Molecular Dynamics Simulation: Elementary Methods*; John Wiley & Sons: New York, 1992.
(29) Résibois, P.; De Leener, M. *Classical Kinetic Theory of Fluids*; Wiley: New York, 1997.
(30) Daivis, P. J.; Evans, D. J. *J. Chem. Phys.* **1995**, *103*, 4261.
(31) (a) Clarke, J. H. R. In *Advances in Infrared and Raman Spectroscopy*; Clark, R. J. H., Hester, R. E., Eds.; Heyden:New York, 1978; Vol. 4. (b) Steele, W. A. In *Spectroscopy and Relaxations in Molecular Liquids*; Steele, D., Yarwood, J., Eds.; Elsevier: Amsterdam, The Netherlands, 1991.
(32) Prystupa, D. A.; Anderson, A, Torrie, B. H. *J. Raman Spectrosc.* **1999**, *20*, 345.
(33) Tironi, I. G.; Van Gunsteren, W. F. *Mol. Phys*. **1994**, *83*, 381.
(34) Glasstone, S.; Laidler, K. J.; Eyring, H. *The Theory of Rate Processes*; McGraw-Hill: New York, 1941.
(35) Anderson, J.; Ullo, J. J.; Yip, S. *J. Chem. Phys.* **1987**, *87*, 1726.
(36) *Handbook of Chemistry and Physics*, 81st ed.; Linde, D. R., Ed.; CRC Press: New York, 2000.
(37) Miller, P. J.; Block, S.; Piermarini, G. J. *J. Phys. Chem*. **1989**, *93*, 462.
(38) Cromer, D. T.; Ryan, R. R.; Schiferl, D. *J. Phys. Chem*. **1985**, *89*, 2315.
(39) Murnaghan, F. D. In *Finite Deformation of an Elastic Solid*; Dover Publications: New York, 1951; p 73.
(40) Pangilinan, G. I.; Gupta, Y. M. *J. Phys. Chem*. **1994**, *98*, 4522.